AGU PUBLICATIONS

Geophysical Research Letters

RESEARCH LETTER
10.1002/2017GL074889

Key Points:
- Urban climate ensemble projections with unprecedented detail demonstrate a heat stress increase twice as large for cities as for rural areas
- Urban heat stress by the mid-21st century is multiplied by a factor 1.4 to 15, depending on the emission and land use scenario
- The urban hot spots of global warming are established by urban heat islands, their concurrence with heat waves, and urban expansion

Supporting Information:
- Supporting Information S1

Correspondence to:
H. Wouters,
Hendrik.Wouters@kuleuven.be

Citation:
Wouters, H., et al. (2017), Heat stress increase under climate change twice as large in cities as in rural areas: A study for a densely populated midlatitude maritime region, *Geophys. Res. Lett.*, *44*, 8997–9007, doi:10.1002/2017GL074889.

Received 14 FEB 2017
Accepted 10 AUG 2017
Published online 7 SEP 2017

Heat stress increase under climate change twice as large in cities as in rural areas: A study for a densely populated midlatitude maritime region

Hendrik Wouters[1,2], Koen De Ridder[3], Lien Poelmans[3], Patrick Willems[4], Johan Brouwers[5], Parisa Hosseinzadehtalaei[4], Hossein Tabari[4], Sam Vanden Broucke[1], Nicole P. M. van Lipzig[1], and Matthias Demuzere[1,2]

[1]Department of Earth and Environmental Sciences, KU Leuven, Heverlee, Belgium, [2]Laboratory of Hydrology and Water Management, Ghent University, Ghent, Belgium, [3]Environmental Modelling Unit, Flemish Institute for Technological Research, Mol, Belgium, [4]Department of Civil Engineering, KU Leuven, Heverlee, Belgium, [5]Flanders Environment Agency, Aalst, Belgium

Abstract Urban areas are usually warmer than their surrounding natural areas, an effect known as the urban heat island effect. As such, they are particularly vulnerable to global warming and associated increases in extreme temperatures. Yet ensemble climate-model projections are generally performed on a scale that is too coarse to represent the evolution of temperatures in cities. Here, for the first time, we combine unprecedented long-term (35 years) urban climate model integrations at the convection-permitting scale (2.8 km resolution) with information from an ensemble of general circulation models to assess temperature-based heat stress for Belgium, a densely populated midlatitude maritime region. We discover that the heat stress increase toward the mid-21st century is twice as large in cities compared to their surrounding rural areas. The exacerbation is driven by the urban heat island itself, its concurrence with heat waves, and urban expansion. Cities experience a heat stress multiplication by a factor 1.4 and 15 depending on the scenario. Remarkably, the future heat stress surpasses everywhere the urban hot spots of today. Our results demonstrate the need to combine information from climate models, acting on different scales, for climate change risk assessment in heterogeneous regions. Moreover, these results highlight the necessity for adaptation to increasing heat stress, especially in urban areas.

1. Introduction

Expanding urban areas are hot spots that drive environmental change at multiple scales around the globe [*Seto et al.*, 2012; *Grimm et al.*, 2008]. Particularly, greenhouse gas emissions and land use changes both lead to global warming and shifts in weather extremes [*Kalnay and Cai*, 2003; *Revi et al.*, 2014] with more intense, more frequent, and longer-lasting heat waves [*Meehl and Tebaldi*, 2004]. The climatic changes are expected to adversely influence the economy, ecosystems, and humans that are exposed to it [*Watts et al.*, 2015; *Revi et al.*, 2014; *Seto et al.*, 2012]. Heat waves particularly result in excessive mortality rates [*Mora et al.*, 2017; *Mazdiyasni et al.*, 2017; *Mitchell et al.*, 2016; *Green et al.*, 2016; *Cox et al.*, 2016; *Xu et al.*, 2016; *Tong et al.*, 2015; *Huang et al.*, 2012], higher hospital admissions [*Linares et al.*, 2017; *Iñiguez et al.*, 2016; *Díaz et al.*, 2015], preterm delivery [*Cox et al.*, 2016], economic and labor productivity loss [*Estrada et al.*, 2017; *Zander et al.*, 2015], damage to infrastructure, and higher energy usage [*Revi et al.*, 2014]. The total death toll by extreme temperatures hitting Europe in Summer 2003 and the Russian Federation in Summer 2010 makes heat waves the second deadliest kind of disaster related to weather extremes during the period 2001 to 2010 [*World Meteorological Organization (WMO)*, 2014]. The cities—housing already more than 50% of the global population [*United Nations*, 2014]—experience an excessive death toll during heat waves compared to the natural surroundings because of the urban heat island (UHI) effect [*Heaviside et al.*, 2016; *Hoag*, 2015; *Watts et al.*, 2015; *Laaidi et al.*, 2011; *Gabriel and Endlicher*, 2011; *Kalnay and Cai*, 2003] and also an excessive economic loss [*Estrada et al.*, 2017].

Recent studies have been using ensemble general circulation models (GCMs) and regional climate models (RCMs) to address the future (heat wave related) risks of climate change around the globe including the role

of urbanization [*Mora et al.*, 2017; *Estrada et al.*, 2017; *Mitchell et al.*, 2016; *Fischer et al.*, 2012; *Taylor et al.*, 2012; *Diffenbaugh and Giorgi*, 2012; *Fischer and Schär*, 2010; *Wilby*, 2008; *Meehl and Tebaldi*, 2004]. However, all of these studies use climate information on a scale (size of grid cells >2500 km^2) that is too coarse to resolve the interurban variability of the cities. In order to capture the associated heterogeneity in urban atmospheric feedbacks, the local circulations and weather conditions, one requires to resolve at least the scale of the cities themselves (<100 km^2). The latter is particularly a prerequisite to distinguish between the cities with different urban characteristics, including the imperviousness (abundance of buildings, streets, parkings, and other man-made water-impermeable pavements) and other local environmental aspects (distance from the coastline, soil texture, orography, etc.). It is also indispensable for taking the local land use change such as urban expansion into account. Convection-permitting models (CPMs; size of grid cells $\leq$25 km^2), offering more than 100 times more grid cells per unit area than those previous assessments, are able to explicitly resolve the local heterogeneous weather conditions and especially the urban heat island effect [e.g., *Trusilova et al.*, 2016; *Jänicke et al.*, 2016; *Wouters et al.*, 2016, 2013; *Bohnenstengel et al.*, 2011; *Van Weverberg et al.*, 2008]. As such, they allow to identify the local hot spots and the associated urban climate change risks [*Prein et al.*, 2015]. Yet CPM downscaling is computationally very expensive, hence recent studies [e.g., *Fosser et al.*, 2017; *Argüeso et al.*, 2015] only consider a limited amount of emission and land use scenarios [*Kendon et al.*, 2017]. As such, they do not provide the statistically robust information and uncertainty regarding the ensemble climate change statistics in weather extremes such as heat waves.

Here we project temperature-based urban heat stress under global warming with a unique combination of CPM urban climate downscaling [*Wouters et al.*, 2016; *Rockel et al.*, 2008], ensemble information from GCMs [*Taylor et al.*, 2012; *Willems and Vrac*, 2011], and sociodemographic land use change modeling [*White and Engelen*, 2000]. The CPM climate simulations are performed covering continuous periods of 35 years over an extended heterogeneous urban area. As such, heat stress is quantified for a historical (1980–2014) and a future (2040–2074) period with different global emission scenarios and local land use scenarios for Belgium, one of the most densely populated and urbanized regions in Europe (The World Bank, 2017, http://data.worldbank.org/indicator/ access date: 2017/03/30). The Belgian scene comprises a compelling case for a midlatitude maritime climate regime with cities of multiple sizes and urban sprawl throughout the domain. It also includes a topographical scene with flatlands in the north, a coastal area in the west, and a hilly area in the south, see Figure S1 in the supporting information. In order to account for the temperature changes and associated uncertainties occurring at the global and local scale, a set of global emission scenarios and local land use change scenarios are considered. A description of the urban climate downscaling, the heat stress indicator, the greenhouse gas emission and land use change scenarios, and the decomposition of the climatic drivers of urban heat stress increase is given in section 2. The results and discussion are presented in sections 3 and 4, respectively. Finally, the implications for policy are provided in section 5.

2. Materials and Methods

2.1. CPM Climate Downscaling

A control experiment for heat stress assessment is obtained from a 35 year (1980–2014) CPM urban climate hindcast simulation with the COSMO-CLM model [*Rockel et al.*, 2008; *Doms et al.*, 2011; *Buzzi*, 2008; *Smiatek et al.*, 2008; *Steppeler et al.*, 2003] coupled to the urban land surface scheme TERRA_URB [*Wouters et al.*, 2015, 2016; *Demuzere et al.*, 2017] configured over Belgium at 2.8 km resolution (Figure S1). The downscaling strategy takes the lateral boundary conditions from the ERA-Interim-driven COSMO-CLM simulation at 12.5 km resolution from the COordinated Regional climate Downscaling EXperiment (CORDEX) for Europe [*Kotlarski et al.*, 2014; *Jacob et al.*, 2013; *Vautard et al.*, 2013]. In agreement to the evaluation of the climate model in earlier studies [*Brisson et al.*, 2016a, 2016b; *Wouters et al.*, 2015, 2016; *Trusilova et al.*, 2016; *Demuzere et al.*, 2017; *Davin et al.*, 2016], the control simulation was found to reproduce both the observed coarse temperature climatology and the urban heat islands of the study domain very well, see Figures S2, S3, S4, and Table S4. A detailed description and evaluation of the urban climate model and its control configuration is provided in the supporting information S1 (see Texts S1 to S4) [*WMO*, 2008; *Davin et al.*, 2016; *Davy and Esau*, 2014; *Jacob et al.*, 2007; *Wouters et al.*, 2013; *Dimitrova et al.*, 2016; *Thiery et al.*, 2016; *Vanden Broucke et al.*, 2015; *Akkermans et al.*, 2014; *Davin et al.*, 2014; *Grossman-Clarke et al.*, 2016; *Prein et al.*, 2013; *Grasselt*, 2008; *Schulz et al.*, 2016; *Haylock et al.*, 2008; *De Ridder et al.*, 2015].

Even though the model has a very good skill in accordance to previous (CPM) model evaluations, the threshold-based heat stress indicator is very sensitive to the model bias. Therefore, a bias correction is applied

according to gridded daily temperature fields and urban climate observations. Details about the bias correction can be found in Text S5. As such, the modeled record of the heat stress indicator matches very well the urban climate observations in Antwerp, especially the urban/rural contrast (see Figure S5).

2.2. Heat Stress Indicator

In order to quantify heat stress for Belgium under climate change, the heat stress indicator from the Flanders Environment Agency is applied. It has been developed in cooperation with several research institutes and governmental agencies regarding climate, care, and health in Belgium. It is used to monitor the potential effect of heat stress episodes on a yearly basis, as a part of the state of the environment reporting in Flanders [see *Brouwers et al.*, 2015; http://www.milieurapport.be]. The heat stress indicator is obtained by summing over the days (i) from the beginning of April until the end of September:

$$\sum_i \left[\left(T_{\mathrm{min},i} - 18.2^{\circ}\mathrm{C}\right)^{+} + \left(T_{\mathrm{max},i} - 29.6^{\circ}\mathrm{C}\right)^{+} \right] h_i \tag{1}$$

On the one hand, the frequency and length of heat waves are considered by means of h_i, which indicates the occurrence of a heat wave day when heat wave alarm levels for temperature are exceeded: It equals to one in case the daily minimum ($T_{\mathrm{min},i}$) and maximum ($T_{\mathrm{max},i}$) temperature simultaneously exceed their respective thresholds 18.2°C and 29.6°C during three consecutive days, whereas it equals to zero for the other days. On the other hand, the intensity of the heat waves is taken into account with the concept of exceeding values of those temperature thresholds. Therefore, the terms in the inner brackets $(\ldots)^{+}$ represent the exceedance of $T_{\mathrm{min},i}$ and $T_{\mathrm{max},i}$ above their respective threshold values 18.2°C and 29.6°C. A motivation of the used heat stress indicator is provided in Text S6.

2.3. Local Land Use Change Scenarios

Two static local land use scenarios are considered for the CPM climate integrations, namely, a historical urbanization (LND:HST; reference year 2000) and a future business-as-usual urbanization (LND:BAU; reference year 2060) [*Acosta-Michlik et al.*, 2011]. They are created using the cellular automata modeling approach [*White and Engelen*, 2000], starting from CORINE land cover data set for the reference year 2000 on a 300 m resolution. The model takes into account the land use changes from the past, while societal boundary conditions with regard to future policy include economic and demographic changes at the different governmental levels. Based on the behavior of pattern changes of land use from the past, a business-as-usual-scenario is obtained. By making an overlay with the existing impervious surface area (abundance of buildings, streets, parkings, and other man-made water-impermeable pavements) from *Maucha et al.* [2010], the land use maps are used for estimating the impervious surface area for the historical and future urbanization, which in turn is taken as input for the CPM climate downscaling. Detailed information can be found in Text S3 (see also Figure S6).

2.4. Global Emission Scenarios

Global emission scenarios are constructed according to the delta change approach [*Tabari et al.*, 2015; *Willems and Vrac*, 2011]. It considers the absolute changes between the temperature distributions from future ensemble scenario runs and those from present-day control runs. Similar as in previous assessment studies [e.g., *Ahlström et al.*, 2012], these are added to the historical time series to obtain the future temperatures. The changes in the 10 category quantiles of the distributions for each month separately of the daily minimum and maximum temperature between the periods 1961–1990 and 2071–2100 are extracted from ensemble GCM data. The changes are rescaled to obtain the results between the periods 1980–2014 and 2040–2074. The ensemble data include 42 simulations comprising 11 control runs and 31 future scenario runs (8 × RCP2.6; 8 × RCP4.5; 6 × RCP6.0; and 9 × RCP8.5; full member list provided in Table S3). These are provided by 11 GCMs from the Coupled Model Intercomparison Project of the World Climate Research Programme Phase 5 (CMIP5) multimodel experiment [*Taylor et al.*, 2012; *Moss et al.*, 2008]. Three scenarios are constructed from this ensemble, namely, the best case (EMI:BEC), the median (EMI:MED), and the worst case (EMI:WOC) scenario. They respectively consider the 5th, 50th, and 95th percentile values of the above mentioned changes, offering the uncertainty range of future temperature changes (see Figures S7a and S7b). The percentile changes are applied to the historical CPM downscaling fields described in section 2.1.

A motivation and interpretation of the global emission scenarios—especially their relation with the different RCP scenarios—are provided in Text S7 of the supporting information (see also Figure S7c).

2.5. Climatic Drivers of Heat Stress Increase

The total heat stress increase under climate change expressed in heat wave degree days (ΔHWDD; see section 2.2) is decomposed [*Stein and Alpert*, 1993] into its different climatic drivers:

$$\begin{aligned}\Delta HWDD_{TOTAL} = {} & \Delta HWDD_{BASE} + \Delta HWDD_{SPD} \\ & + \Delta HWDD_{CPM\_M} + \Delta HWDD_{CPM\_TD} \\ & + \Delta HWDD_{CPM\_LUC} + \Delta HWDD_{SPD,CPM}\end{aligned} \quad (2)$$

The BASEline term (BASE) indicates the change according to the ensemble global emission scenarios (section 2.4) by changing the monthly-mean temperatures of the coarse-scale record of gridded observations by *Haylock et al.* [2008] (see Figure S7a). The Shifting Probability Distribution term (SPD) refers to the additional heat stress increase when also taking into account the differential change in the monthly 10-category quantiles of the daily minimum and maximum temperature distributions (section 2.4; see Figure S7b). The contribution of urban heat stress increase related to the CPM downscaling (section 2.1) is quantified by subsequently adding the monthly-mean CPM (fine-scale) temperature deviation from the above coarse-scale observational record (CPM_MD), the inclusion of the day-to-day time dependency of the CPM temperatures (CPM_TD), and the inclusion of the future local land use change under a business-as-usual scenario (CPM_LUC; see section 2.3). Finally, the additional covariance term (SPD,CPM) arises from simultaneously providing the information about the shifting probability distribution and the CPM downscaling.

3. Results

3.1. Historical Heat Stress

Results for the heat stress indicator (section 2.2) based on the present-day climate information (section 2.1) from the CPM downscaling are presented below. Substantial temporal variation of annual-based historical heat stress is found (Figure S8): excessive heat stress is perceived for the heat wave years (1994, 1995, 2003, 2006, 2010, 2012, and 2013), whereas it vanishes for other years. For the years of extreme heat between 2001 to 2010, Belgium recorded an excessive heat wave-related mortality rate of 4200 people (http://www.milieurapport.be). On the European scale, the death toll for the heat wave of 2003 have surpassed 70,000 [*Barriopedro et al.*, 2011]. A strong spatial variation of the heat stress is found as well. The city centers experience on average 17 heat wave degree days on an annual basis on average (see Figure 1), whereas periurban and rural areas only experience 12 and 2.6 days, respectively. As such, cities experience much higher heat stress than their respective natural surroundings, which is caused by the UHI effect. UHI intensities increase with city size (expressed in population number) and imperviousness [*Zhou et al.*, 2013]; hence, the relation is also found for urban heat stress in the current results (compare Antwerp and Ghent in Figure S8). Inland cities experience larger heat stress than cities of comparable size closer to the coastline (compare Hasselt with Bruges in Figure S8). The hilly rural areas with the higher elevation levels in the south experience less heat stress compared to the lower rural flatlands in the north. Yet the cities centers in the south still experience similar or even higher heat stress as in the north, because they are located more inland and at low elevation levels in the river valleys (compare Liège with Ghent).

3.2. Heat Stress Projections

On the basis of local land use change scenarios described in section 2.3 and global emission scenarios described in section 2.4, future heat stress projections are presented below. The role of the global emission scenarios is larger than the role of local land use change scenarios in terms of the overall heat stress increase under global warming and its spread for Belgium (Figures 1 and 2). On average, the heat stress in the urban centers is multiplied by a factor ranging from 1.5 to 15 depending on the emission scenario, considering the business-as-usual land use change scenario. These increase factors become slightly smaller when the land use change is not taken into account (between 1.4 and 14). Similar to the historical heat stress, the future heat stress has a strong spatial variation. The hot spots are found in the urban centers experiencing an absolute increase of the annual heat stress from 6.0 to 237 heat wave degree days, and these hot spots become more intense away from the coastline. For the periurban areas and rural areas, the absolute increase is much smaller from 4.7 to 207 and from 2.2 and 143 heat wave degree days, respectively. As such, the absolute heat stress increase is about twice as large for the city centers as for the natural surroundings (urban increment factor between 1.7 and 2.7 considering the different scenarios). The heat stress in the future climate in case of the

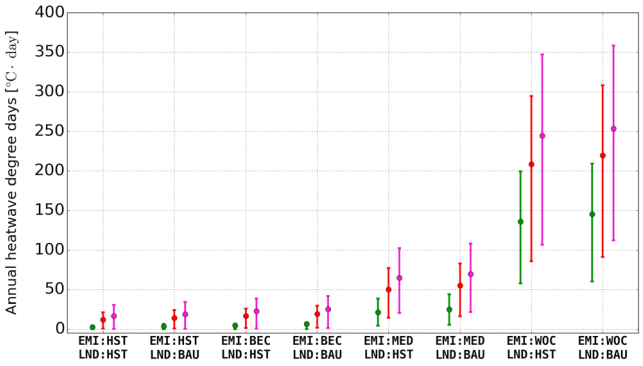

Figure 1. Climate downscaling hindcast (1980–2014) and projections (2040–2074) of heat stress for Belgium based on the ensemble emission scenarios (EMI:HiSTorical/EMI:BEst-Case/EMI:MEDian/EMI:WOrst-Case) and land use change scenarios (LND:HiSTorical/LND:Business-As-Usual) for different urban classes. The results are averaged for different levels of impervious surface area fraction (ISA), i.e., urban centers (purple; ISA for the surrounding 100 km^2 $\geq$ 50%), periurban areas (red; 25% $\leq$ ISA (100 km^2) < 50%) and rural areas (green; ISA (100 km^2) < 25%). The bullets show the climatological mean, whereas the error bars show the climatological spread calculated from the range between the 5th and 95th percentile. An overview of the different scenarios are listed in Table S2, and their description (including the urban climate downscaling methodology and the used heat stress indicator) can be found in section 2.

median and worst case emission scenarios largely exceeds the heat stress during the extreme years (i.e., the 95th percentile value of the annual heat stress) in the current climate. In addition, the heat stress for the rural areas in the future climate is higher than that for the cities in the current climate. Remarkably, the future heat stress for the worst case emission scenario in the rural areas during the coldest years exceeds the present-day heat stress in the urban centers during the hottest years.

3.3. Climatic Drivers

The presented scenarios allow for a decomposition of the different climatic drivers of heat stress increase occurring at the different scales. The decomposition follows the methodology described in section 2.5 and the results are shown in Figure 3. A substantial part of the heat stress increase is explained by the global warming trends in the GCMs imposed on coarse-scale gridded observational records. Herein, both the monthly mean change (BASE) and the shifting probability distribution (SPD) of the daily temperatures are important. The latter stems from the shifting trends in high-temperature extremes in the global emission scenarios, especially in the worst case scenario (see Figure S7b), for which an excessive increase of high extremes of daily temperatures is found with respect to the averaged temperatures increase.

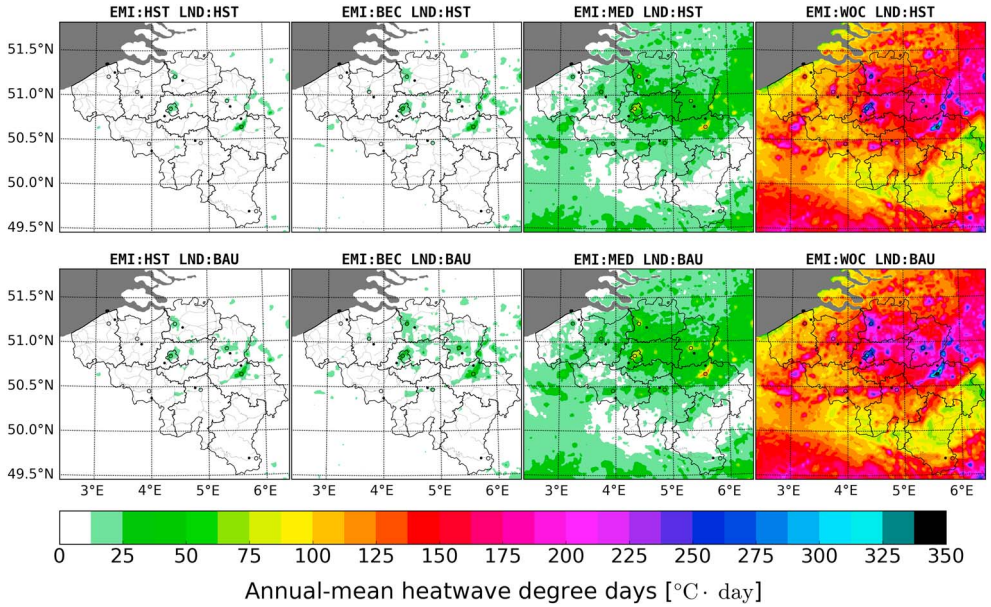

Figure 2. Climate downscaling hindcast (1980–2014) and projections (2040–2074) of annual-mean heat stress based on the (top row) global emission scenarios (EMI:HiSTorical/EMI:BEst-Case/EMI:MEDian/EMI:WOrst-Case) and (bottom row) local land use change scenarios (LND:HiSTorical/LND:Business-As-Usual) over Belgium. The heat stress is expressed in heat wave degree days according to the heat stress indicator provided in section 2.2. An overview of the different scenarios are listed in Table S2, and their description can be found in sections 2.3 and 2.4. The center of Brussels and the provincial capitals are indicated with circles.

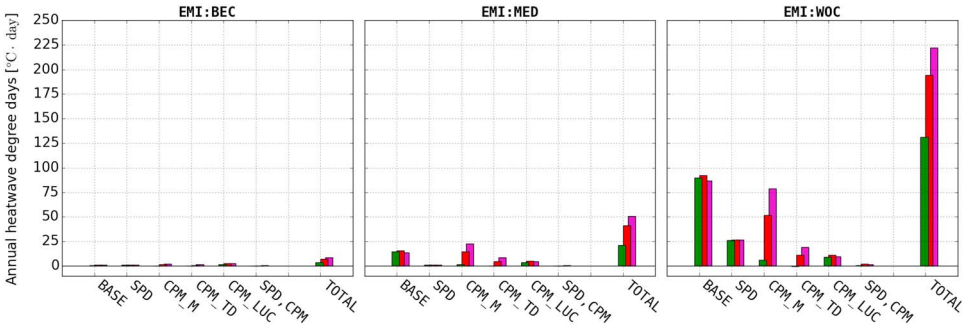

Figure 3. Total heat stress increase (TOTAL) and its climatic drivers under the three global emission scenarios (EMI:HiSTorical/EMI:BEst-Case/EMI:MEDian/EMI:WOrst-Case), expressed in future change in annual heat wave degree days (°C day). Results are averaged for different levels of impervious surface area fractions, i.e., urban centers (purple; Impervious Surface Area (ISA) for the surrounding 100 km^2 $\geq$ 50%), periurban areas (red; 25% $\leq$ ISA (100 km^2) $<$ 50%) and rural areas (green; ISA (100 km^2) $<$ 25%). The drivers consist of the baseline increase (BASE), the shifting probability distribution (SPD), the annual-mean contribution from the convection-permitting model downscaling (CPM_M), its day-to-day time dependency (CPM_TD), the local land use change (CPM_LUC), and finally the covariance between shifting probability distribution and the CPM downscaling information (SPD,CPM). Details about the emission scenarios and the decomposition of the climatic drivers can be found in sections 2.4 and 2.5, respectively.

This is in agreement with the expected increase in temperature variance for Western Europe [*Vogel et al.*, 2017; *Horton et al.*, 2015; *Donat and Alexander*, 2012; *Schär et al.*, 2004; *Beniston et al.*, 2007; *Seneviratne et al.*, 2006]. We reveal a profound exacerbation of heat stress increase by the CPM climate downscaling. In the urban centers, the exacerbation ranges between 96% and 381% relative to the GCM-based trends depending on the emission scenario. Particularly, cities already experiencing higher temperatures due to the UHI effect perceive an additional heat stress increase under global warming. We find that the major part of this excess is attributed to urban heat islands on a monthly basis (CPM_M). However, we demonstrate that the day-to-day variation of the CPM downscaling leads to an important additional excess as well (CPM_TD) and results from the excessive UHI intensities during heat waves [*Hamdi et al.*, 2016; *Li and Bou-Zeid*, 2013]. In fact, the high-pressure conditions with high surface solar irradiation and low wind speeds establishing heat waves also enhance urban heat island intensities [*De Ridder et al.*, 2016]. The terms CPM_M and CPM_TD denote the additional heat stress increase under climate change resulting from the higher temperatures—especially during heat waves—in the cities than in the rural areas. Such an excessive heat stress increase originates from the nonlinear response of the heat stress (indicator) to increasing temperatures (taking both the number and intensity of heat wave days into account) occurring at the global and synoptic scale.

Finally, a further excess in heat stress results from the local land use change by urban expansion (CPM_LUC) for the three urban categories. It mostly affects the periurban areas where the urban expansion typically takes place, yet it also affects the city centers. Here an excess accumulation takes place in the periurban areas around the city centers; At night, the air in the direction of the urban centers accumulates more heat (or is cooled less) due to the increasing amount of heat stored in the cities' periphery. This eventually leads to a greater UHI intensity in the centers. While the additional effect from urban expansion seems small, the overall heat stress increase is found to be twice as large in urban areas compared to that in the rural areas. This is not contradicting: in the former, the effect of urban expansion does not reflect (yet accounts for) the effect of existing urbanization. In the latter, the heat stress increase also considers the effect of existing urbanization. Furthermore, additional future urban heat stress increase established by local land use change averaged for the three urban categories may seem small compared to that established by the global emissions on the scale of the study domain. Still, this further exacerbation may have important consequences for the city centers in the median and worst case emission scenarios. Moreover, it should be noted that new emerging urban areas experience strong impacts as their future heat stress becomes more similar to the existing urban areas (compare Figure 2, bottom row with Figure 2, top row), particularly the new urban sprawl around Brussels and Antwerp in the center of the domain.

4. Discussion

Our results are consistent with previous heat stress assessments which also found a profound heat stress increase in response to greenhouse gas-induced climate change [*Fischer and Schär*, 2010; *Meehl and Tebaldi*, 2004; *Huth et al.*, 2000], and an amplification by the expanding urban land forms [*Argüeso et al.*, 2015; *Fischer et al.*, 2012]. They support the view that there will be a strong increase in the risk of heat wave-related problems, especially for citizens' mortality because of more extreme future heat waves [*Mora et al.*, 2017; *Wilby*, 2008]. However, the new framework, that combines climate models acting on the different scales, offers novel insights on the relation between heat wave-related problems, urbanization, and climate change and are summarized below:

1. By explicitly resolving the interurban heterogeneity, the urban CPM reveals the propagation of heat stress increase under climate change toward the scales of the cities. It also indicates its dependency to the city size and imperviousness and to other local environmental aspects such as distance from the coastline, soil texture, and orography. As such, local hot spots of heat stress are identified and, particularly, the role of urban heat islands and their concurrence with heat waves. Moreover, our modeling approach reveals the additional role of local land use change indicating that urban expansion results in a further amplification of heat stress increase under climate change.
2. The incorporation of the ensemble information from the GCMs allows us to quantify the climatic drivers of heat stress at the global and synoptic scale, especially the role of the trends in both averaged and extreme temperature.
3. The combination of the ensemble global emission scenarios and local land use change scenarios enables a comprehensive quantification of the different heat stress drivers under climate change at the global to the local scale. This includes the characterization of the uncertainty ranging from a best- case to a worst case global emission scenario.

While the urban heat stress drivers and the underlying mechanisms are explained for a specific region, their implications are relevant for other regions around the world. Particularly, the majority of cities are susceptible to global warming and UHIs, which could lead to comparable climate drivers of heat stress as those found for the current study area. Still, this needs to be verified with additional climate assessments.

Our study further exemplifies that the model framework—especially urban CPM—holds great promise for urban climate assessment with respect to other regions and other risks related to climate change. Especially, one should consider the (sub)tropic developing regions for which urban expansion and population growth are expected to be much larger than in midlatitude developed regions [*United Nations*, 2014; *Seto et al.*, 2012]. Besides the heat stress assessment, the framework may also serve as a basis for assessing other weather extremes and risks under climate change propagating to the city scales, especially urban-induced precipitation [e.g., *Han et al.*, 2014; *Jin et al.*, 2015] and its consequences on urban flooding and (vector-borne) diseases. Still, limitations of the current assessment need to be kept in mind with respect to the heat stress quantification (Text S8.1), urban climate observations, modeling and projections (Text S8.2), and land use modeling (Text S8.3). Especially, one should keep in mind that our study employs projected temperature changes derived from ensemble GCM simulations, for which changes in the local (city-scale) feedbacks and other meteorological variables for heat stress quantification are neglected. The challenges need to be tackled with new research directions and modeling techniques, which are discussed further in the supporting information Text S8 [*Mora et al.*, 2017; *Leutwyler et al.*, 2016; *Xu et al.*, 2016; *Buzan et al.*, 2015; *Hondula et al.*, 2014; *Wouters et al.*, 2013; *Bohnenstengel et al.*, 2011; *Barnett et al.*, 2010; *Matzarakis et al.*, 2010; *Epstein and Moran*, 2006].

5. Implications for Policy

Our study highlights that one requires combined measures of heat-resistance and sustainability against global warming, especially in urban areas. Especially, the quantification of the different heat stress drivers under climate change demonstrate that adaptation and mitigation strategies should come together:

1. From a global perspective, mitigating the global heat stress drivers requires drastic reduction of greenhouse gas emissions in systems for energy, housing, industry, food, movables, and mobility.
2. From a regional perspective, one should prioritize those strategies that also mitigate the local drivers by reducing the urban heat island effect. Particularly, the transformation of the urban areas into compact

cities with a low-carbon infrastructure [*Creutzig et al.*, 2016; *Seto et al.*, 2010] (reducing the motorized traffic, building energy consumption, and petrified footprint) will alleviate the heat stress increase not only from greenhouse gas emissions but also that from urban expansion and anthropogenic heating.

3. From a local perspective, the future heat stress drivers highlight the need for targeted strategies in spatial, organizational, behavioral, and technological climate adaptation [*Hanna and Tait*, 2015; *Revi et al.*, 2014; *Georgescu et al.*, 2014] that enhance the cities' resilience to a changing climate and attractiveness. Such adaptation includes the integration of green open spaces and waterways in urban spatial planning, water-sensitive urban design, and building adaptation [*Demuzere et al.*, 2014; *Coutts et al.*, 2012; *Willems et al.*, 2012].

Interdisciplinary research needs to pursue optimal pathways for future urbanization, for which heat-reducing strategies apply to the multiple scales of climate change, on the one hand, and of policy making, on the other hand. It is clear from our study that urban convection-permitting models should serve as a key tool.

Acknowledgments

We acknowledge the World Climate Research Programme's Working Group on Coupled Modeling, which is responsible for CMIP, and we thank the climate modeling groups (listed in Table S3 in the supporting information) for producing and making available their model output. For CMIP the U.S. Department of Energy's Program for Climate Model Diagnosis and Intercomparison provides coordinating support and leads development of software infrastructure in partnership with the Global Organization for Earth System Science Portals. We also acknowledge the CLM community for the developing COSMO-CLM model, and for providing the model code and the CORDEX-Europe boundary conditions. In addition, we are grateful to the World Climate Research Programme (WRCP) for initiating and coordinating the CORDEX-Europe initiative, ECMWF for providing access to the ERA-Interim data set, the EU-FP6 project ENSEMBLES (http://ensembles-eu.metoffice.com), and the data providers in the ECA&D project (http://www.ecad.eu) for making the E-OBS data set publicly available. We particularly thank Bino Maiheu for coordinating the urban climate observations for Antwerp and Ghent, and for providing the data. The work described in this paper has received funding from the Belgian Science Policy Office through its Science for a Sustainable Development Programme under contracts SD/CS/041/MACCBET and BR/143/A2/CORDEX.be. It has also received funding from the Flemish Government through a contract as an FWO (Fund for Scientific Research) postdoctoral position, and from the EU-H2020 programme through the "BRIGAID - BRIdges the GAp for Innovations in Disaster resilience" project. The computational resources and services used for the downscaling were provided by the Hercules Foundation and the Flemish Government (department of Economics, Sciences and Innovation-EWI). We are thankful to the reviewers for their constructive comments, which have considerably improved the quality of the manuscript. The climate data can be requested through the CORDEX.be project portal (http://www.euro-cordex.be).

References

Acosta-Michlik, L., H. B. de Frahan, H. Brunke, K. Hansen, G. Engelen, I. Uljee, A. Van Herzele, M. Rounsevell, and R. White (2011), Multiscalar and multiagent modelling framework for assessing sustainable futures in a globalised environment (MULTIMODE, Final Report), *Tech. Rep.*, Belgian Science Policy, Research Programme Science for a Sustainable Development, Brussels.

Ahlström, A., G. Schurgers, A. Arneth, and B. Smith (2012), Robustness and uncertainty in terrestrial ecosystem carbon response to CMIP5 climate change projections, *Environ. Res. Lett.*, *7*(4), 44008, doi:10.1088/1748-9326/7/4/044008.

Akkermans, T., W. Thiery, and N. P. M. Van Lipzig (2014), The regional climate impact of a realistic future deforestation scenario in the Congo basin, *J. Clim.*, *27*(7), 2714–2734, doi:10.1175/JCLI-D-13-00361.1.

Argüeso, D., J. P. Evans, A. J. Pitman, and A. Di Luca (2015), Effects of city expansion on heat stress under climate change conditions, *PloS One*, *10*(2), e0117066, doi:10.1371/journal.pone.0117066.

Barnett, A., S. Tong, and A. Clements (2010), What measure of temperature is the best predictor of mortality?, *Environ. Res.*, *110*(6), 604–611, doi:10.1016/j.envres.2010.05.006.

Barriopedro, D., E. M. Fischer, J. Luterbacher, R. M. Trigo, and R. García-Herrera (2011), The hot summer of 2010: Redrawing the temperature record map of Europe, *Science*, *332*(6026), 220–224.

Beniston, M., et al. (2007), Future extreme events in European climate: An exploration of regional climate model projections, *Clim. Change*, *81*(S1), 71–95, doi:10.1007/s10584-006-9226-z.

Bohnenstengel, S. I., S. Evans, P. A. Clark, and S. Belcher (2011), Simulations of the London urban heat island, *Q. J. R. Meteorol. Soc.*, *137*(659), 1625–1640, doi:10.1002/qj.855.

Brisson, E., M. Demuzere, and N. P. van Lipzig (2016a), Modelling strategies for performing convection-permitting climate simulations, *Meteorol. Z.*, *25*(2), 149–163, doi:10.1127/metz/2015/0598.

Brisson, E., K. Van Weverberg, M. Demuzere, A. Devis, S. Saeed, M. Stengel, and N. P. M. van Lipzig (2016b), How well can a convection-permitting climate model reproduce decadal statistics of precipitation, temperature and cloud characteristics?, *Clim. Dyn.*, *47*, 3043–3061, doi:10.1007/s00382-016-3012-z.

Brouwers, J., et al. (2015), MIRA Climate Report 2015, about observed and future climate changes in Flanders and Belgium, *Tech. Rep.*, Flanders Environment Agency in collaboration with KU Leuven, VITO and RMI, Aalst, Belgium.

Buzan, J. R., K. Oleson, and M. Huber (2015), Implementation and comparison of a suite of heat stress metrics within the Community Land Model version 4.5, *Geosci. Model Dev.*, *8*(2), 151–170, doi:10.5194/gmd-8-151-2015.

Buzzi, M. (2008), Challenges in operational numerical weather prediction at high resolution in complex terrain, *PhD thesis*, ETH, Zürich, Switzerland, doi:10.3929/ethz-a-005698833.

Coutts, A. M., N. J. Tapper, J. Beringer, M. Loughnan, and M. Demuzere (2012), Watering our cities: The capacity for water sensitive urban design to support urban cooling and improve human thermal comfort in the Australian context, *Prog. Phys. Geogr.*, *37*(1), 2–28, doi:10.1177/0309133312461032.

Cox, B., A. Gasparrini, B. Catry, A. Delcloo, E. Bijnens, J. Vangronsveld, and T. S. Nawrot (2016), Mortality related to cold and heat. What do we learn from dairy cattle?, *Environ. Res.*, *149*, 231–238, doi:10.1016/j.envres.2016.05.018.

Creutzig, F., P. Agoston, J. C. Minx, J. G. Canadell, R. M. Andrew, C. L. Quéré, G. P. Peters, A. Sharifi, Y. Yamagata, and S. Dhakal (2016), Urban infrastructure choices structure climate solutions, *Nat. Clim. Change*, *6*(12), 1054–1056, doi:10.1038/nclimate3169.

Davin, E. L., S. I. Seneviratne, P. Ciais, A. Olioso, and T. Wang (2014), Preferential cooling of hot extremes from cropland albedo management, *Proc. Natl. Acad. Sci. U.S.A.*, *111*(27), 9757–9761, doi:10.1073/pnas.1317323111.

Davin, E. L., E. Maisonnave, and S. I. Seneviratne (2016), Is land surface processes representation a possible weak link in current regional climate models?, *Environ. Res. Lett.*, *11*(7), 74027, doi:10.1088/1748-9326/11/7/074027.

Davy, R., and I. Esau (2014), Global climate models' bias in surface temperature trends and variability, *Environ. Res. Lett.*, *9*(11), 114024, doi:10.1088/1748-9326/9/11/114024.

De Ridder, K., D. Lauwaet, and B. Maiheu (2015), UrbClim—A fast urban boundary layer climate model, *Urban Clim.*, *12*, 21–48, doi:10.1016/j.uclim.2015.01.001.

De Ridder, K., B. Maiheu, D. Lauwaet, I. Daglis, I. Keramitsoglou, K. Kourtidis, P. Manunta, and M. Paganini (2016), Urban heat island intensification during hot spells—The case of Paris during the summer of 2003, *Urban Sci.*, *1*(1), 3, doi:10.3390/urbansci1010003.

Demuzere, M., A. Coutts, M. Göhler, A. Broadbent, H. Wouters, N. van Lipzig, and L. Gebert (2014), The implementation of biofiltration systems, rainwater tanks and urban irrigation in a single-layer urban canopy model, *Urban Clim.*, *10*, 148–170, doi:10.1016/j.uclim.2014.10.012.

Demuzere, M., S. Harshan, L. Järvi, M. Roth, C. Grimmond, V. Masson, K. Oleson, E. Velasco, and H. Wouters (2017), Impact of urban canopy models and external parameters on the modelled urban energy balance in a tropical city, *Q. J. R. Meteorol. Soc.*, *143*, 1581–1596, doi:10.1002/qj.3028.

Díaz, J., R. Carmona, I. Mirón, C. Ortiz, and C. Linares (2015), Comparison of the effects of extreme temperatures on daily mortality in Madrid (Spain), by age group: The need for a cold wave prevention plan, *Environ. Res.*, *143*, 186–191, doi:10.1016/j.envres.2015.10.018.

Diffenbaugh, N. S., and F. Giorgi (2012), Climate change hotspots in the CMIP5 global climate model ensemble, *Clim. Change*, *114*(3–4), 813–822, doi:10.1007/s10584-012-0570-x.

Dimitrova, R., Z. Silver, T. Zsedrovits, C. M. Hocut, L. S. Leo, S. Di Sabatino, and H. J. S. Fernando (2016), Assessment of planetary boundary-layer schemes in the weather research and forecasting mesoscale model using MATERHORN field data, *Boundary Layer Meteorol.*, *159*(3), 589–609, doi:10.1007/s10546-015-0095-8.

Doms, G., J. Förstner, E. Heise, H.-J. Herzog, M. Raschendorfer, T. Reinhardt, T. Ritter, R. Schrodin, J.-P. Schulz, and G. Vogel (2011), *A Description of the Nonhydrostatic Regional COSMO Model. Part II: Physical Parameterization*, 153 pp., Deutscher Wetterdienst, Offenbach, Germany.

Donat, M. G., and L. V. Alexander (2012), The shifting probability distribution of global daytime and night-time temperatures, *Geophys. Res. Lett.*, *39*, L14707, doi:10.1029/2012GL052459.

Epstein, Y., and D. S. Moran (2006), Thermal comfort and the heat stress indices, *Indust. Health*, *44*(3), 388–98.

Estrada, F., W. J. W. Botzen, and R. S. J. Tol (2017), A global economic assessment of city policies to reduce climate change impacts, *Nat. Clim. Change*, *7*(6), 403–406, doi:10.1038/nclimate3301.

Fischer, E. M., and C. Schär (2010), Consistent geographical patterns of changes in high-impact European heatwaves, *Nat. Geosci.*, *3*(6), 398–403, doi:10.1038/ngeo866.

Fischer, E. M., K. W. Oleson, and D. M. Lawrence (2012), Contrasting urban and rural heat stress responses to climate change, *Geophys. Res. Lett.*, *39*, L03705, doi:10.1029/2011GL050576.

Fosser, G., S. Khodayar, and P. Berg (2017), Climate change in the next 30 years: What can a convection-permitting model tell us that we did not already know?, *Clim. Dyn.*, *48*(5-6), 1987–2003, doi:10.1007/s00382-016-3186-4.

Gabriel, K. M. a., and W. R. Endlicher (2011), Urban and rural mortality rates during heat waves in Berlin and Brandenburg, Germany, *Clim. Dyn.*, *159*(8-9), 2044–2050, doi:10.1016/j.envpol.2011.01.016.

Georgescu, M., P. E. Morefield, B. G. Bierwagen, and C. P. Weaver (2014), Urban adaptation can roll back warming of emerging megapolitan regions, *Proc. Natl. Acad. Sci. U.S.A.*, *111*(8), 2909–14, doi:10.1073/pnas.1322280111.

Grasselt, R. (2008), Validation of TERRA-ML with discharge measurements, *Meteorol. Z.*, *17*(6), 763–773, doi:10.1127/0941-2948/2008/0334.

Green, H. K., N. Andrews, B. Armstrong, G. Bickler, and R. Pebody (2016), Mortality during the 2013 heatwave in England—How did it compare to previous heatwaves? A retrospective observational study, *Environ. Res.*, *147*, 343–349, doi:10.1016/j.envres.2016.02.028.

Grimm, N. B., S. H. Faeth, N. E. Golubiewski, C. L. Redman, J. Wu, X. Bai, and J. M. Briggs (2008), Global change and the ecology of cities, *Science*, *319*(5864), 756–760, doi:10.1126/science.1150195.

Grossman-Clarke, S., S. Schubert, and D. Fenner (2016), Urban effects on summertime air temperature in Germany under climate change, *Int. J. Climatol.*, *37*, 905–917, doi:10.1002/joc.4748.

Hamdi, R., F. Duchêne, J. Berckmans, A. Delcloo, C. Vanpoucke, and P. Termonia (2016), Evolution of urban heat wave intensity for the Brussels Capital Region in the ARPEGE-Climat A1B scenario, *Urban Clim.*, *17*, 176–195, doi:10.1016/j.uclim.2016.08.001.

Han, J.-Y., J.-J. Baik, and H. Lee (2014), Urban impacts on precipitation, *Asia-Pacific J. Atmos. Sci.*, *50*(1), 17–30, doi:10.1007/s13143-014-0016-7.

Hanna, E. G., and P. W. Tait (2015), Limitations to thermoregulation and acclimatization challenge human adaptation to global warming, *Int. J. Environ. Res. Public Health*, *12*(7), 8034–8074, doi:10.3390/ijerph120708034.

Haylock, M. R., N. Hofstra, A. M. G. Klein Tank, E. J. Klok, P. D. Jones, and M. New (2008), A European daily high-resolution gridded data set of surface temperature and precipitation for 1950–2006, *J. Geophys. Res.*, *113*, D20119, doi:10.1029/2008JD010201.

Heaviside, C., S. Vardoulakis, and X.-M. Cai (2016), Attribution of mortality to the urban heat island during heatwaves in the West Midlands, UK, *Environ. Health*, *15*(1), S27, doi:10.1186/s12940-016-0100-9.

Hoag, H. (2015), How cities can beat the heat, *Nature*, *524*(7566), 402–404, doi:10.1038/524402a.

Hondula, D. M., M. Georgescu, and R. C. Balling (2014), Challenges associated with projecting urbanization-induced heat-related mortality, *Sci. Total Environ.*, *490*, 538–544, doi:10.1016/j.scitotenv.2014.04.130.

Horton, D. E., N. C. Johnson, D. Singh, D. L. Swain, B. Rajaratnam, and N. S. Diffenbaugh (2015), Contribution of changes in atmospheric circulation patterns to extreme temperature trends, *Nature*, *522*(7557), 465–469, doi:10.1038/nature14550.

Huang, C., A. G. Barnett, X. Wang, and S. Tong (2012), The impact of temperature on years of life lost in Brisbane, Australia, *Nat. Clim. Change*, *2*(4), 265–270, doi:10.1038/nclimate1369.

Huth, R., J. Kyselý, and L. Pokorná (2000), A GCM simulation of heat waves, dry spells, and their relationships to circulation, *Clim. Change*, *46*(1/2), 29–60, doi:10.1023/A:1005633925903.

Iñiguez, C., P. Schifano, F. Asta, P. Michelozzi, A. Vicedo-Cabrera, and F. Ballester (2016), Temperature in summer and children's hospitalizations in two Mediterranean cities, *Environ. Res.*, *150*, 236–244, doi:10.1016/j.envres.2016.06.007.

Jacob, D., et al. (2007), An inter-comparison of regional climate models for Europe: Model performance in present-day climate, *Clim. Change*, *81*(S1), 31–52, doi:10.1007/s10584-006-9213-4.

Jacob, D., et al. (2013), EURO-CORDEX: New high-resolution climate change projections for European impact research, *Regional Environ. Change*, *14*(2), 563–578, doi:10.1007/s10113-013-0499-2.

Jänicke, B., F. Meier, D. Fenner, U. Fehrenbach, A. Holtmann, and D. Scherer (2016), Urban-rural differences in near-surface air temperature as resolved by the Central Europe Refined analysis (CER): Sensitivity to planetary boundary layer schemes and urban canopy models, *Int. J. Climatol.*, *37*, 2063–2079, doi:10.1002/joc.4835.

Jin, M., Y. Li, and D. Su (2015), Urban-induced mechanisms for an extreme rainfall event in Beijing China: A satellite perspective, *Climate*, *3*(1), 193–209, doi:10.3390/cli3010193.

Kalnay, E., and M. Cai (2003), Impact of urbanization and land-use change on climate, *Nature*, *423*(6939), 528–531, doi:10.1038/nature01675.

Kendon, E. J., et al. (2017), Do convection-permitting regional climate models improve projections of future precipitation change? *Bull. Am. Meteorol. Soc.*, *98*(1), 79–93, doi:10.1175/BAMS-D-15-0004.1.

Kotlarski, S., et al. (2014), Regional climate modeling on European scales: A joint standard evaluation of the EURO-CORDEX RCM ensemble, *Geosci. Model Dev.*, *7*(4), 1297–1333, doi:10.5194/gmd-7-1297-2014.

Laaidi, K., A. Zeghnoun, B. Dousset, P. Bretin, and S. Vandentorren (2011), The impact of Heat Islands on mortality in Paris during the August 2003 heatwave, *Environ. Health Perspect.*, *120*(2), 254–259, doi:10.1289/ehp.1103532.

Leutwyler, D., O. Fuhrer, X. Lapillonne, D. Lüthi, and C. Schär (2016), Towards European-scale convection-resolving climate simulations with GPUs: A study with COSMO 4.19, *Geosci. Model Dev.*, *9*(9), 3393–3412, doi:10.5194/GMD-9-3393-2016.

Li, D., and E. Bou-Zeid (2013), Synergistic interactions between urban heat islands and heat waves: The impact in cities is larger than the sum of its parts, *J. Appl. Meteorol. Climatol.*, *52*, 2051–2064, doi:10.1175/JAMC-D-13-02.1.

Linares, C., D. Culqui, R. Carmona, C. Ortiz, and J. Díaz (2017), Short-term association between environmental factors and hospital admissions due to dementia in Madrid, *Environ. Res.*, *152*, 214–220, doi:10.1016/j.envres.2016.10.020.
Matzarakis, A., F. Rutz, and H. Mayer (2010), Modelling radiation fluxes in simple and complex environments: Basics of the RayMan model, *Int. J. Biometeorol.*, *54*(2), 131–139, doi:10.1007/s00484-009-0261-0.
Maucha, G., G. Büttner, and B. Kosztra (2010), European validation of GMES FTS soil sealing enhancement data, final draft, *Tech. Rep.*, Eur. Environ. Agency, Copenhagen, Denmark.
Mazdiyasni, O., A. AghaKouchak, S. J. Davis, S. Madadgar, A. Mehran, E. Ragno, M. Sadegh, A. Sengupta, S. Ghosh, C. T. Dhanya, and M. Niknejad (2017), Increasing probability of mortality during Indian heat waves, *Sci. Adv.*, *3*(6), e1700066.
Meehl, G. A., and C. Tebaldi (2004), More intense, more frequent, and longer lasting heat waves in the 21st century, *Science*, *305*(5686), 994–997.
Mitchell, D., C. Heaviside, S. Vardoulakis, C. Huntingford, G. Masato, B. P Guillod, P. Frumhoff, A. Bowery, D. Wallom, and M. Allen (2016), *Environ. Res. Lett.*, *11*(7), 74006, doi:10.1088/1748-9326/11/7/074006.
Mora, C., et al. (2017), Global risk of deadly heat, *Nat. Clim. Change*, *7*, 501–506, doi:10.1038/nclimate3322.
Moss, R., N. Nakicenovic, and B. O'Neill (2008), *Towards New Scenarios for Analysis of Emissions, Climate Change, Impacts, and Response Strategies*, IPCC, Geneva.
Prein, A. F., A. Gobiet, M. Suklitsch, H. Truhetz, N. K. Awan, K. Keuler, and G. Georgievski (2013), Added value of convection permitting seasonal simulations, *Clim. Dyn.*, *41*(9-10), 2655–2677, doi:10.1007/s00382-013-1744-6.
Prein, A. F., et al. (2015), A review on regional convection-permitting climate modeling: Demonstrations, prospects, and challenges, *Rev. Geophys.*, *53*, 323–361, doi:10.1002/2014RG000475.
Revi, A., D. E. Satterthwaite, F. Aragón-Durand, J. Corfee-Morlot, R. B. R. Kiunsi, M. Pelling, D. C. Roberts, and W. Solecki (2014), Urban areas, in *Climate Change 2014: Impacts, Adaptation, and Vulnerability. Part A: Global and Sectoral Aspects. Contribution of Working Group II to the Fifth Assessment Report of the Intergovernmental Panel of Climate Change*, edited by C. B. Field et al., pp. 535–612, Cambridge Univ. Press, Cambridge, U. K., and New York.
Rockel, B., A. Will, and A. Hense (2008), The regional climate model COSMO-CLM (CCLM), *Meteorol. Z.*, *17*(4), 347–348.
Schär, C., P. L. Vidale, D. Lüthi, C. Frei, C. Häberli, M. A. Liniger, and C. Appenzeller (2004), The role of increasing temperature variability in European summer heatwaves, *Nature*, *427*(6972), 332–336, doi:10.1038/nature02300.
Schulz, J.-P., G. Vogel, C. Becker, S. Kothe, U. Rummel, and B. Ahrens (2016), Evaluation of the ground heat flux simulated by a multi-layer land surface scheme using high-quality observations at grass land and bare soil, *Meteorol. Z.*, *25*, 607–620, doi:10.1127/metz/2016/0537.
Seneviratne, S. I., D. Lüthi, M. Litschi, and C. Schär (2006), Land-atmosphere coupling and climate change in Europe, *Nature*, *443*(7108), 205–209, doi:10.1038/nature05095.
Seto, K. C., R. Sánchez-Rodríguez, and M. Fragkias (2010), The New Geography of Contemporary Urbanization and the Environment, *Annu. Rev.*, *35*, 167–194, doi:10.1146/annurev-environ-100809-125336.
Seto, K. C., B. Güneralp, and L. R. Hutyra (2012), Global forecasts of urban expansion to 2030 and direct impacts on biodiversity and carbon pools, *Proc. Natl. Acad. Sci. U.S.A.*, *109*(40), 16,083–16,088, doi:10.1073/pnas.1211658109.
Smiatek, G., B. Rockel, and U. Schättler (2008), Time invariant data preprocessor for the climate version of the COSMO model (COSMO-CLM), *Meteorol. Z.*, *17*(4), 395–405, doi:10.1127/0941-2948/2008/0302.
Stein, U., and P. Alpert (1993), Factor separation in numerical simulations, *J. Atmos. Sci.*, *50*, 2107–2115.
Steppeler, J., G. Doms, U. Schättler, H. W. Bitzer, A. Gassmann, U. Damrath, and G. Gregoric (2003), Meso-gamma scale forecasts using the nonhydrostatic model LM, *Meteorol. Atmos. Phys.*, *82*(1-4), 75–96, doi:10.1007/s00703-001-0592-9.
Tabari, H., M. T. Taye, and P. Willems (2015), Water availability change in central Belgium for the late 21st century, *Global Planet. Change*, *131*, 115–123, doi:10.1016/j.gloplacha.2015.05.012.
Taylor, K. E., R. J. Stouffer, and G. A. Meehl (2012), An overview of CMIP5 and the experiment design, *Bull. Am. Meteorol. Soc.*, *93*(4), 485–498, doi:10.1175/BAMS-D-11-00094.1.
Thiery, W., E. L. Davin, S. I. Seneviratne, K. Bedka, S. Lhermitte, and N. P. M. van Lipzig (2016), Hazardous thunderstorm intensification over Lake Victoria, *Nat. Commun.*, *7*, 12786, doi:10.1038/ncomms12786.
Tong, S., G. FitzGerald, X.-Y. Wang, P. Aitken, V. Tippett, D. Chen, X. Wang, and Y. Guo (2015), Exploration of the health risk-based definition for heatwave: A multi-city study, *Environ. Res.*, *142*, 696–702, doi:10.1016/j.envres.2015.09.009.
Trusilova, K., S. Schubert, H. Wouters, B. Früh, S. Grossman-Clarke, M. Demuzere, and P. Becker (2016), The urban land use in the COSMO-CLM model: A comparison of three parameterizations for Berlin, *Meteorol. Z.*, *25*(2), 231–244, doi:10.1127/metz/2015/0587.
United Nations (2014), World Urbanization Prospects: The 2014 Revision, *Tech. Rep. ST/ESA/SER.A/366*, U.N., Dep. of Econ. and Soc. Affairs, Popul. Div., New York.
Van Weverberg, K., K. De Ridder, and A. Van Rompaey (2008), Modeling the contribution of the Brussels Heat Island to a long temperature time series, *J. Appl. Meteor. Climatol.*, *47*, 976–990, doi:10.1175/2007JAMC1482.1.
Vanden Broucke, S., S. Luyssaert, E. L. Davin, I. Janssens, and N. van Lipzig (2015), New insights in the capability of climate models to simulate the impact of LUC based on temperature decomposition of paired site observations, *J. Geophys. Res. Atmos.*, *120*, 5417–5436, doi:10.1002/2015JD023095.
Vautard, R., et al. (2013), The simulation of European heat waves from an ensemble of regional climate models within the EURO-CORDEX project, *Clim. Dyn.*, *41*(9-10), 2555–2575, doi:10.1007/s00382-013-1714-z.
Vogel, M. M., R. Orth, F. Cheruy, S. Hagemann, R. Lorenz, B. J. J. M. Hurk, and S. I. Seneviratne (2017), Regional amplification of projected changes in extreme temperatures strongly controlled by soil moisture-temperature feedbacks, *Geophys. Res. Lett.*, *44*, 1511–1519, doi:10.1002/2016GL071235.
Watts, N., et al. (2015), Health and climate change: Policy responses to protect public health, *The Lancet*, *386*(10006), 1861–1914, doi:10.1016/S0140-6736(15)60854-6.
White, R., and G. Engelen (2000), High-resolution integrated modelling of the spatial dynamics of urban and regional systems, *Comput. Environ. Urban Syst.*, *24*(5), 383–400, doi:10.1016/S0198-9715(00)00012-0.
Wilby, R. L. (2008), Constructing climate change scenarios of urban heat island intensity and air quality, *Environ. Planning B*, *35*(5), 902–919, doi:10.1068/b33066t.
Willems, P., and M. Vrac (2011), Statistical precipitation downscaling for small-scale hydrological impact investigations of climate change, *J. Hydrol.*, *402*(3), 193–205, doi:10.1016/j.jhydrol.2011.02.030.
Willems, P., J. Olsson, K. Arnbjerg-Nielsen, S. Beecham, A. Pathirana, I. B. Gregersen, and H. Madsen (2012), *Impacts of Climate Change on Rainfall Extremes and Urban Drainage Systems*, 238 pp., The Int. Water Assoc., London.
World Meteorological Organization (WMO) (2008), *Guide to Meteorological Instruments and Methods of Observation*, 7th ed., 681 pp., World Meteorol. Organ., Geneva, Switzerland.

World Meteorological Organization (WMO) (2014), *Atlas of Mortality and Economic Losses from Weather, Climate and Water Extremes 1970-2012*, World Meteorol. Organ., Geneva, Switzerland.

Wouters, H., K. De Ridder, M. Demuzere, D. Lauwaet, and N. P. M. van Lipzig (2013), The diurnal evolution of the urban heat island of Paris: A model-based case study during Summer 2006, *Atmos. Chem. Phys.*, *13*(17), 8525–8541, doi:10.5194/acp-13-8525-2013.

Wouters, H., M. Demuzere, K. De Ridder, and N. P. van Lipzig (2015), The impact of impervious water-storage parametrization on urban climate modelling, *Urban Clim.*, *11*, 24–50, doi:10.1016/j.uclim.2014.11.005.

Wouters, H., M. Demuzere, U. Blahak, K. Fortuniak, B. Maiheu, J. Camps, D. Tielemans, and N. P. M. van Lipzig (2016), The efficient urban canopy dependency parametrization (SURY) v1.0 for atmospheric modelling: Description and application with the COSMO-CLM model for a Belgian summer, *Geosci. Model Dev.*, *9*(9), 3027–3054, doi:10.5194/gmd-9-3027-2016.

Xu, Z., G. FitzGerald, Y. Guo, B. Jalaludin, and S. Tong (2016), Impact of heatwave on mortality under different heatwave definitions: A systematic review and meta-analysis, *Environ. Int.*, *89*, 193–203, doi:10.1016/j.envint.2016.02.007.

Zander, K. K., W. J. W. Botzen, E. Oppermann, T. Kjellstrom, and S. T. Garnett (2015), Heat stress causes substantial labour productivity loss in Australia, *Nat. Clim. Change*, *5*(7), 647–651, doi:10.1038/nclimate2623.

Zhou, B., D. Rybski, and J. P. Kropp (2013), On the statistics of urban heat island intensity, *Geophys. Res. Lett.*, *40*, 5486–5491, doi:10.1002/2013GL057320.